Blasting seismographs: Transfer functions, standards and accuracy

P. Segarra[1], J.A. Sanchidrián[1], I. del Castillo[2], R. Castedo[1], L.M. López[1] & J. Navarro[1]

[1]Universidad Politécnica de Madrid – E.T.S.I. Minas y Energía
[2]Vibraquipo

Abstract

In this work a blasting seismograph was tested on a vibration shaker controlled by a single-point laser Doppler vibrometer (LDV). A total of 43 tests were made to measure the transfer properties (transmissibility and phase shift) of the basic elements of the full monitoring chain and investigate the performance of the full system. The main elements of the seismograph are described by second order transfer functions with typical parameters calibrated through nonlinear fit of the measured responses. The resulting transfer function is used to compare the behavior of the tested seismograph with four theoretical seismographs representative of those used in blasting. Fifteen theoretical inputs are run through the transfer function of each seismograph to assess their steady-response. The error (expressed as gain) in the peak velocity has been assessed. It varies from -1.5 to 2.3 dB (equivalent to a transmissibility of 0.84 to 1.3, respectively) depending on the seismograph and frequencies of the input. The largest errors occurred for input signals with frequencies in the low (<32 Hz) or high ranges (>125 Hz), where the mechanical, electronics and digital parts of the seismograph modify the signals. Seismographs with the nominal transfer function described by DIN 45669:1:2010 are ranked with the smallest errors. Monitoring devices with transmissibility around one in a narrow bandwidth, in line with ISEE suggested criteria for amplitude response, involve large phase shifts at low and high frequencies, resulting in a worst performance.

Introduction

Digital seismographs are the most common vibration monitoring system used to assess compliance of vibrations from blasting with existing damage prevention criteria (AENOR, 1993; BSI, 1993; DIN, 1999; Siskind et al., 1980). They are composed by three orthogonally oriented sensors placed in a metallic case and connected to a recording-processing unit. The response of the seismograph (including the geophones and the processing unit) to the incoming ground motion is described by the complex frequency response or by its mathematical equivalent, transfer function (Wielandt, 2002). These are generally given as curves of the amplitude response (or transmissibility) and phase shift versus frequency. Transmissibility is the modulus of the frequency response showing at each frequency the factor by which the input is modified, whereas the phase response is the argument and gives the time shift between the output and input signals.

The measurement of the phase shift on a vibration shaker by comparison to a reference transducer requires the same source of time for the system under calibration and the reference transducer (see ISO 16063-21:2003). This is not a problem when the sensor is investigated alone as was made for geophones used in blasting by Farnfield (1996). But is more complicated when the phase response of the sensor and the processing unit is examined together. DIN standard (2010) and US Geological Survey (Hutt et al., 2009) force to measure the phase shift only in the primary or type (classification) tests to confirm that the requirements of the monitoring device have been meet. Monitoring transmissibility is simpler, as it can be carried out without connecting the seismograph and the reference transducer to the same data acquisition system. It has been measured for various seismographs (Fogelson and Johnson, 1962; Segarra et al. 2015a, b; Stagg and Engler, 1980), but the phase response has not, as far as we know.

The seismographs used nowadays are qualified according to ISEE (2011) or German DIN 45669:1:2010 (2010) specifications. ISEE define tolerance bounds of the transmissibility of the apparatus as function of frequency, whereas the phase shift is only defined in terms of the maximum error produced in the peak particle velocity. DIN standard (2010), with a more general scope than blasting, provides the nominal transfer function of the seismograph, so both amplitude and phase responses are well defined. This information is usually provided for the devices used in seismological stations (Nanometrics, 2009; Nofal et al., 2015; Ueno et al., 2015), but has been little investigated for the whole seismograph. This prevents removing the instrument response from the signal or comparing the seismograph performance with design characteristics without measuring the phase response of the system.

Experiments and instrumentation

The experimental set-up used to measure the response of a seismograph (identified as S0) is shown in Figure 1 (left graph). The geophone's case was directly anchored to the vibration shaker. A hex lag bolt with a reflective adhesive on its head was set between both sensors to measure the velocity of the shaker motion with a laser Doppler vibrometer (LDV). The signal from the LDV is fed back to the vibration controller to correct, if necessary, the driven signal supplied to the exciter.

The shaker table was set to vibrate under a vertical harmonic motion of constant amplitude of 10 mm/s (0.4 in/s) and single frequency; vibrations in the horizontal plane were discarded to minimize tilt-induced errors (Hutt et al., 2009). The frequency of the input motion was varied from 2 to 256 Hz at intervals of 1/6 of octave in 43 tests. An additional test was made at 315 Hz to investigate the response at very high frequencies which may occur when vibrations are monitored at very close distances to the blast (Dowding et al., 2016).

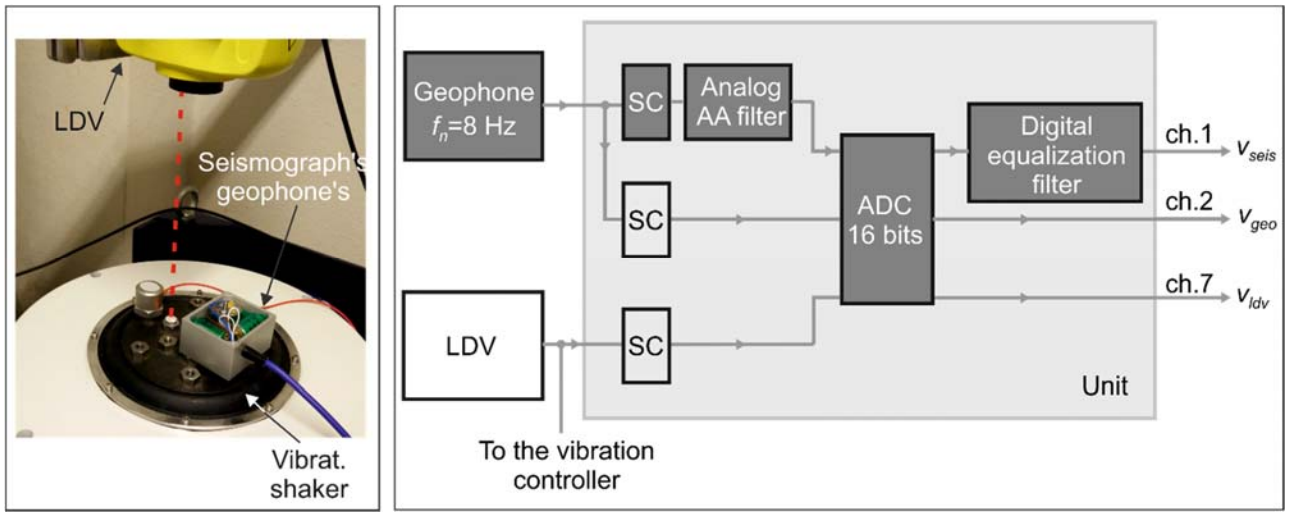

Figure 1. Experimental layout (left) and flowsheet of seismograph S0 (right); f_n is natural frequency, SC signal conditioner, AA anti-aliasing, ADC analog to digital converter.

The LDV and the vertical geophone (the two horizontal geophones were disabled to avoid cross-talk on the vertical geophone) were connected to the digital unit of the seismograph S0 that processes and records the signals from both sensors. The flowsheet of the complete monitoring chain is shown in Figure 1 (right graph). The unit has a range of ±200 mm/s, a resolution of 0.006 mm/s and a sampling rate of 2048 Hz.

In each test, the seismograph was triggered manually once the driven and control signals of the exciter converge. The unit stopped recording vibrations automatically 8 s later.

The output from the vertical geophone was fed into channels 1 and 2. In the later the processing elements were set to a minimum: signal conditioner and an analog to digital converter (ADC). No aliasing is expected for the frequencies investigated (i.e. the highest frequency investigated is well below the Nyquist frequency, 1024 Hz), and no anti-aliasing filter was used in channel 2 to ensure that the output from this channel is essentially the geophone response (v_{geo}). Channel 1 includes all the processing stages typical of modern seismographs to modify the frequency response of the geophone (that we thus called v_{seis}). These stages are colored in dark in the right graph, Figure 1, and are: an analog anti-aliasing filter, the ADC, and the digital equalization filter. The later stage is implemented in a vast majority of seismographs using electronic active circuits before the ADC.

The recording unit was adapted to record the signal from the LDV in channel 7 (v_{ldv}), so the geophone and the LDV have the same time origin. This channel, as with channel 2, is composed by the signal conditioner and the ADC.

Results

All the signals were processed to remove offset. The steady-state complex response to a long enough input signal of a linear-time invariant system, like a geophone or a seismograph, is calculated as the ratio between the discrete Fourier transform of the output and the discrete Fourier transform of the input. These are for the geophone and seismograph, respectively:

$$H_{geo} = V_{geo} / V_{ldv} \quad \text{and} \quad H_{seis} = V_{seis} / V_{ldv} \qquad \text{Equations 1 and 2}$$

where V_{geo}, V_{seis} and V_{ldv} are the discrete fast Fourier transforms of the signals recorded in the tests at each excitation frequency (the same subscripts used for the waveforms, right graph in Figure 1, are considered, but the lowercase v is replaced by an uppercase). The imposed motion is described from the output of channel 7 (v_{ldv} or V_{ldv}) as in all the tests the frequency of this signal is the same than the excitation frequency, and its peak velocity differs from the nominal (10 mm/s or 0.4 in/s) by less than 1.2 % (the overall expanded uncertainty of the testing procedure considering other sources, can be fixed roughly, as 1.5 %).

Figure 2 shows the complex frequency responses of the geophone (top graphs) and seismograph (lower graphs) using Equations 1 and 2, respectively; the amplitude or transmissibility is shown in left graphs and the phase shift in the right ones. At a given frequency, transmissibility above one indicates that the input is amplified, and values below one involves damping. The same sign criteria for the phase shift that it is used in earthquake engineering (Havskow and Alguacil, 2002) is considered here, and negative phases means a delay or a time-shift to the right as considered; phases of $\pm 0.5\pi$ and $\pm\pi$ indicate that the signals are in quadrature and completely out of phase with different polarity, respectively.

The behaviour of the geophone at its natural frequency (8 Hz), with a transmissibility of 0.7 (upper-left graph, Figure 2) and a phase shift of $-\pi/2$ (upper-right graph, Figure 2), is in line with typical values for this sensor (Telford et al., 1990). In order to show the effect of this sensor in the recorded waveform, the signals measured by the geophone and the LDV in tests at the band limits investigated are plotted, as an example, in Figure 3. It shows that vibrations of 2 Hz are strongly damped by the geophone (transmissibility of 0.06) that also shifts the output forward by 218 ms (i.e. $\phi/(2\pi f_m)$, ϕ being the phase and

f_m the frequency, 0.88π and 2 Hz, respectively). At 315 Hz, distortion is limited, being the amplitudes of both signals and their relative position similar; top graphs in Figure 2 shows that transmissibility at such frequency is almost one (0.96) and that the phase shift is close to zero (the time shift is less than 1 ms). Although the sampling rate (2048 Hz) exceeds the minimum values suggested by DIN 45669:1:2010 (630 Hz or twice the maximum frequency expected) and ISEE (1000 Hz), less points are sampled at high frequencies (5-6 points at 315 Hz) resulting in slightly flattened peaks, while the other characteristic, such as the frequency, are not modified.

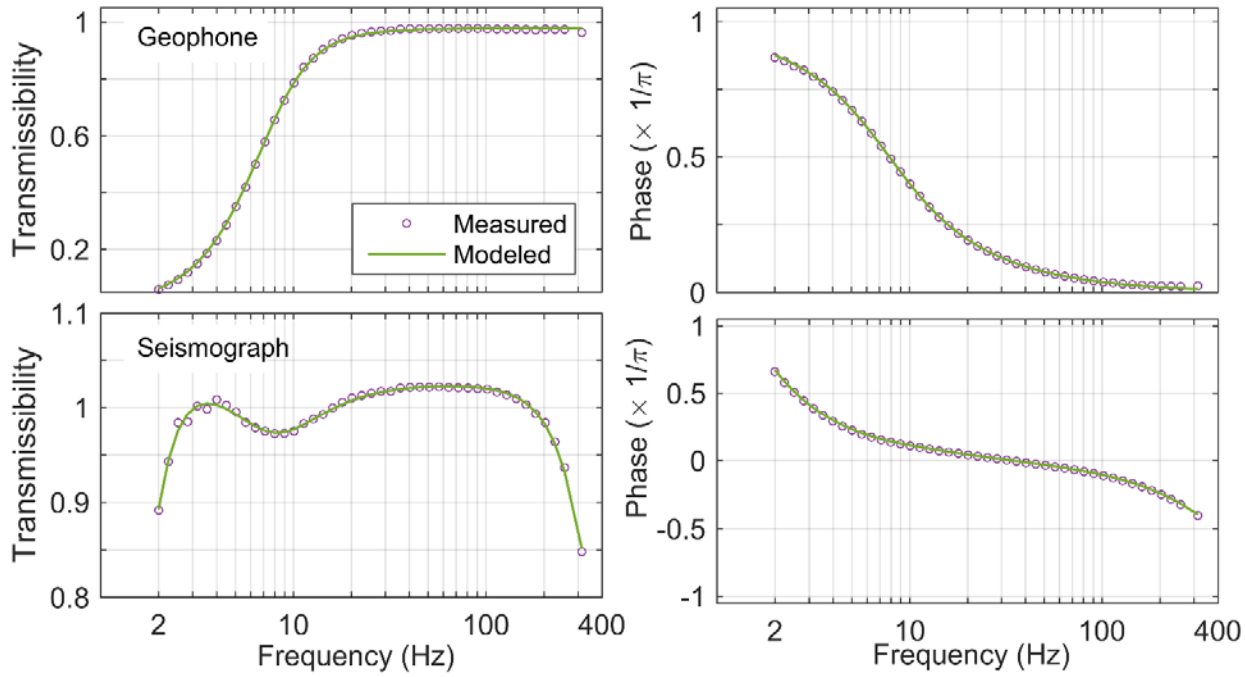

Figure 2. Complex frequency responses of the geophone and seismograph S0; circles are measured data and line is the modeled response with the fitted transfer function (Equation 3).

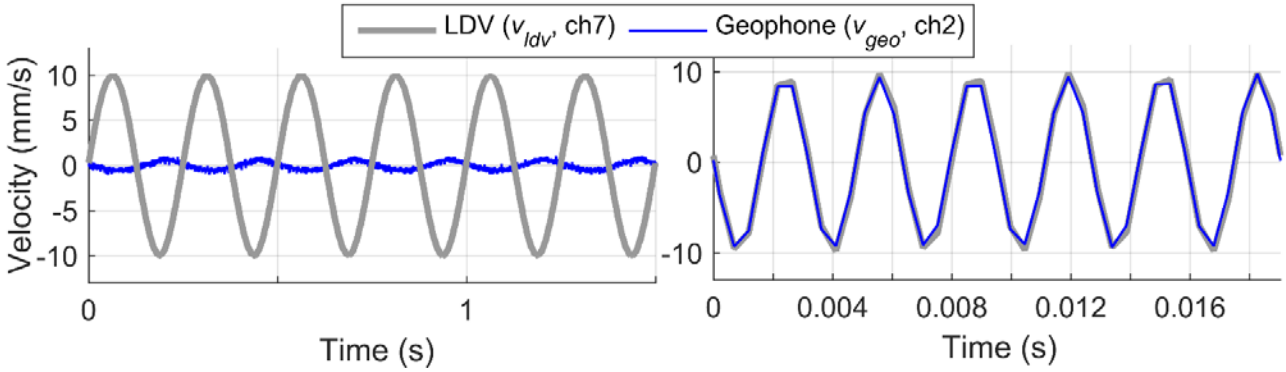

Figure 3. Waveforms from the geophone and the LDV from tests at 2 Hz (left) and 315 Hz (right)

The electronics and digital parts of the seismograph (channel 1; right graph, Figure 1) modify the geophone response (lower graphs, Figure 2). The bandwidth with transmissibility around one is extended down to 2.5 Hz and damping is only 0.9 at 2 Hz. In the high frequency range, transmissibility decays and it is 0.85

at 315 Hz. The phase response is completely different; it is positive at low frequencies, around zero with a linear decreasing trend between 10 and 100 Hz, and negative at high frequencies.

The transfer function

Single-input single-output blocks are used to describe the main elements of the seismograph, namely: geophone, anti-aliasing filter and equalization filter (right graph, Figure 1). The ADC is not modelled because it processes the signals from all channels, and its effect in H_{geo} and H_{seis} is cancelled, see Equations 1 and 2.

A system, such as the seismograph, with an analog input and a digital output can be described with either discrete time or continuous time transform functions (Chen, 1995). In this work, continuous-time (Laplace) functions are considered in line with the analytical description of the nominal seismograph in DIN standard 45669-1:2010. The transfer function of the seismograph is given by:

$$H_{sys}(s) = A_{0g} A_{0p} \prod_{b=1}^{n} H_b(s) \qquad \text{Equation 3}$$

where s is the complex frequency $j\omega$, A_{0g} and A_{0p} are the geophone and processing unit factors or static magnifications that shift upwards or downwards the modeled transmissibility without affecting the phase response, n is the number of blocks, and H_b the transfer function of each block. These are described by second order low-pass or high-pass filters (LPF and HPF filters, respectively) with cut-off frequency ω_0 ($2\pi f_0$) and damping ratio ξ:

$$H_{LPF}(s) = \frac{{\omega_0}^2}{s^2 + 2\xi\omega_0 s + {\omega_0}^2} \quad \text{and} \quad H_{HPF}(s) = \frac{s^2}{s^2 + 2\xi\omega_0 s + {\omega_0}^2} \qquad \text{Equations 4 and 5}$$

The characteristics of each block and the connections between them are shown in Figure 4 (the element modeled by each block is given in the top part and the function used in the center). The geophone is modeled as a high pass filter, HPF (Drijkoningen, 2003; Havskov and Alguacil, 2014; Udías et al., 2014), and the processing unit with four blocks. A low pass filter, LPF, is used to prevent aliasing and define amplitude response at high frequencies according to the specifications followed by the seismograph (ISEE in this case). Two high pass filters and one inverse high pass filter (obtained as the inverse of Equation 5 and identified as HPF^{-1}) are considered to amplify the geophone signal at low frequencies. These three equalization filters are programmed in practice in the unit using a different topology to allow faster calculations.

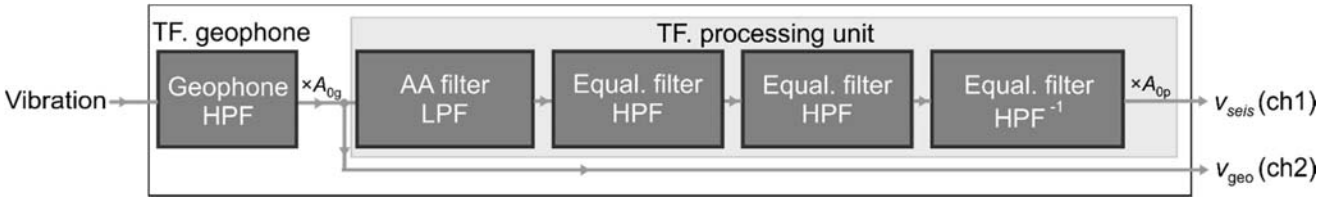

Figure 4. Block diagram of the tested seismograph S0.

The parameters of the geophone are calibrated first from the measured frequency response H_{geo}. The resulting function is applied to get the parameters of the processing unit using the seismograph response H_{seis}. In both cases, MATLAB (2015) software is used running several minimizations to avoid local minima. The fact that the expected corner frequencies of the high-pass and the anti-aliasing filters are outside the bandwidth investigated (2–315 Hz) makes necessary to account for both the modulus and the

argument of the empirical complex frequency response in the function that has been minimized. Otherwise and as transmissibility and the phase response are linked through the transfer function, it would be enough to account only for transmissibility. The modeled frequency responses are plotted with a line in Figure 2; they provide an excellent description of the vibration monitoring chain with determination coefficients above 0.99. The resulting model parameters are shown in the first row of Table 1.

Table 1. Parameters of the tested seismograph (S0) and parameters varied in the other considered seismographs (S1, S2, S3 and S_{DIN})

	Processing unit										
	Geophone			Anti-aliasing filter		Equalization Filters					
						HP filters[a]			Inv. HP filter		A_{0p}
	f_0	ξ	A_{0g}	f_0	ξ	f_0	ξ_1	ξ_2	f_0	ξ	
S0	**7.9**	**0.75**	**0.97**	**397**	**0.72**	**1.4**	**0.56**	**0.81**	**7.9**	**0.71**	**1.05**
S1	=	=	=	=	=	1.5↑	=	0.61↓	7.5↓	0.73↑	=
S2	=	=	=	260↓	0.68↓	1.1↓	=	0.83↑	8.3↑	0.74↑	0.99↓
S3	4.5↓	=	1.02↑	470↑	=	0.7↓	0.45↓	0.90↑	4.5↓	=	1.00↓
S_{DIN}[b]	0.8↓	0.71↓	1.00↑	394↓	0.71↓	×[c]	×	×	×	×	1.00↓

[a] f_0 refers to the corner frequency of each high pass filter, and ξ_1 and ξ_2 to their respective damping ratios.
[b] The transfer function is built with one high-pass filter and one low-pass filter in cascade, and the elements that are not accounted have been disabled (this is shown with a cross symbol[c]).

The resulting cutoff frequency of the geophone-HPF is in good agreement with the actual frequency of the sensor. The damping ratio defined by mechanical and electrical elements of the geophone (Havskov and Alguacil, 2004) agrees with the typical values (around 0.7) that maximize the bandwidth with transmissibility close to one (Telford et al., 1990). The geophone factor A_{0g} of 0.97 defines transmissibility values at high frequencies.

The simulated complex frequency response of the shaping filters in the processing unit from 0.1 to 400 Hz is shown in Figure 5; transmissibility is shown in the left graph and phase response in the right graph. The empirical performance of the unit obtained from the ratio of the measured responses H_{seis} / H_{geo} is also plotted for comparison. Transmissibility is above one, and thus vibrations are amplified, in the bandwidth 0.2–20 Hz. This is achieved by reversing the geophone performance in the inverse high pass filter which corner frequency f_0 and damping ratio ξ are very similar to those of the geophone. The two high pass filters with the same corner frequency and different damping, prevent DC offset and drift of signals over time, and compensate the amplification caused by the inverse filter HPH^{-1} (the left graph in Figure 5 shows that transmissibility is maxima at their natural frequency, 1.4 Hz).

Transmissibility in the passband of the unit (25–100 Hz) is governed by the amplification factor A_{0p} (1.05). The effect of the anti-aliasing LPF filter starts at 100 Hz as can be seen from the change in both the amplitude and phase responses in Figure 5. It damps the input motion by a factor 0.15 at the Nyquist frequency (1024 Hz). The processing unit introduces in the signal from the geophone a nonlinear phase shift (right graph, Figure 5). The main variation occurs in the working range of the two high pass equalization filters at frequencies below their cut-off frequency, 1.4 Hz. Above this frequency, the phase becomes negative and it varies in a tighter range, between -0.1π to -0.5π. The smaller phase shift occurs in the passband 20–100 Hz.

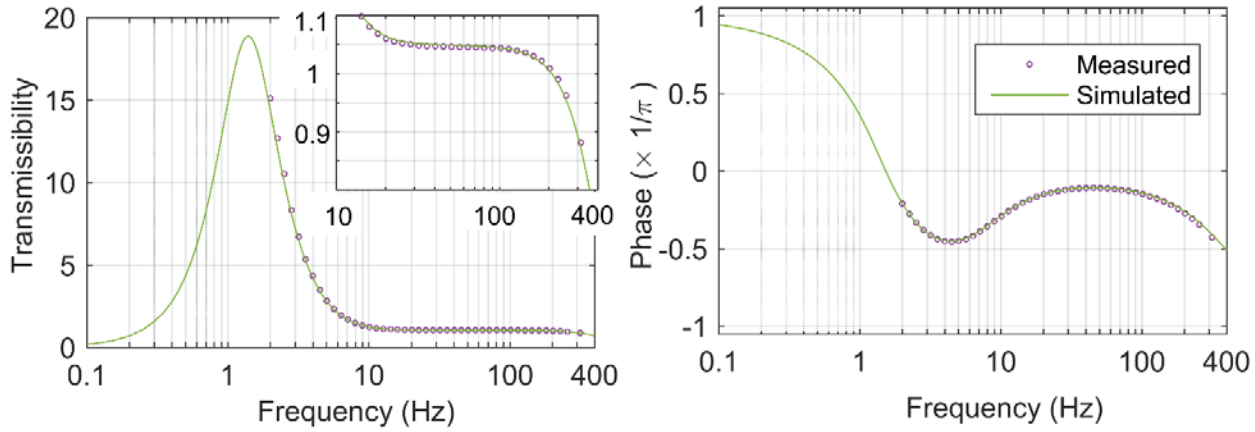

Figure 5. Complex frequency response of shaping filters in the processing unit; transmissibility is shown in the left graph (data in the bandwidth 10–400 Hz is zoomed in and given in the upper left corner) and the phase in the right graph.

Practical implications. Assessment of measuring errors

The transfer function of a seismograph is helpful to obtain the complex frequency response of the system for a given set of parameters. Figure 6 compares the response of the tested seismograph (S0) from 0.5 to 400 Hz with three theoretical seismographs (identified as S1, S2 and S3) modeled with the same transfer function but with different parameters. These are shown in Table 1; an equal symbol shows that the parameter is the same than in seismograph S0, whereas the new value accompanied by an up/down arrow indicates a change. In the case that these seismographs were manufactured, some of the changes carried out would involve hardware modifications, while others would only involve software coding. One additional seismograph (coded as S_{DIN}), following the nominal transfer function suggested by DIN (2010) is also examined.

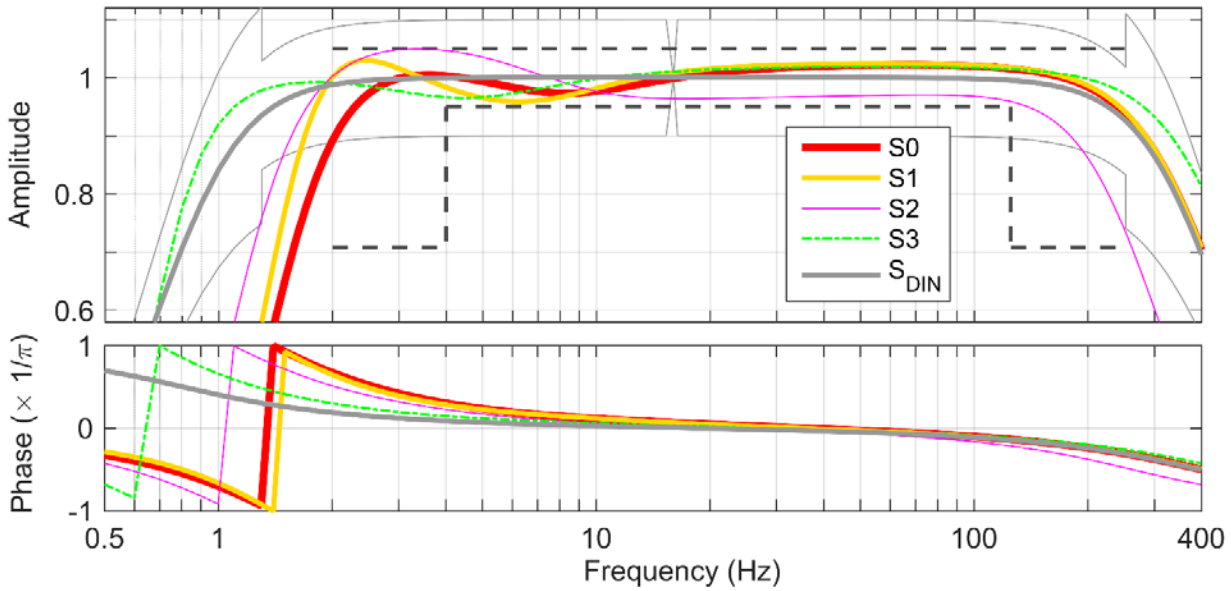

Figure 6. Complex frequency response for five seismographs which typical parameters are shown in Table 1; transmissibility is given in the upper graph (solid grey lines are DIN limits and dashed grey lines are ISEE bounds) and phase shift in the lower.

The aim of the changes implemented in the seismograph parameters is that the resulting devices have different phase responses, while transmissibility is in compliance with ISEE (seismographs S1 and S2) and DIN (seismograph S3) specifications; the transmissibility bounds defined by both standards are plotted as a reference in the upper graph of Figure 6 (the upper limit for ISEE is unclear for frequencies outside 4–125 Hz, and a value of 1.05 has been assumed). The amplitude response of S_{DIN} is near one in the passband 2–180 Hz, whereas the equalization filters of the other devices cause oscillations in transmissibility around one at low frequencies (upper graph, Figure 6). Seismograph S_{DIN} leads to the flattest phase response curve with values close to zero from 3 to 100 Hz (lower graph, Figure 6). The largest phase shifts are obtained with seismographs S0 and S1 at low frequencies, and with S3 in the high frequency range; the jump observed in the phase response for seismographs S0 to S3 occurs at the corner frequency of the high pass equalization filters.

The performance of these seismographs is assessed using as inputs two linearly superimposed harmonics of the same amplitude and frequencies ω_1 and $r\omega_1$, r being an integer. Although this signal type does not describe vibrations from blasting, it is usually considered by DIN (2010) and ISEE (2011) to assess the phase response of seismographs. A total of 15 theoretical signals are considered. Their frequencies are given in the abscissa of Figure 7, and consist on 10 fundamental frequencies from 2 to 125 Hz, and their second or third harmonic (only these harmonics are considered because the effect of the phase delay on the peak velocity of the resulting signal decreases for higher orders). The logarithmic errors in the peak velocity expressed as gain are calculated as follows:

$$e = 20\log_{10}\left(ppv_{out} / ppv_{in}\right) \qquad \text{Equation 6}$$

and ppv_{out} is obtained from the steady-state response of each seismograph to the input signal.

The resulting errors for the five seismographs and the 15 signals considered are shown in Figure 7. They correspond, likely, to the minimum expected errors as larger deviations will likely occur with non-harmonic vibrations (DIN, 2010). The error varies from -1.5 to 2.3 dB (i.e. transmissibility of 0.84 to 1.3) depending on the seismograph and frequencies of the input. The mean errors for each seismograph are given in the legend of Figure 7; these values are calculated as the mean of the absolute value of the errors from all the signals examined. Seismographs S_{DIN} and S3 with an extended bandpass towards low frequencies and thus a flatter phase response (upper and lower graphs, Figure 6) are ranked with the smallest errors; the performance of S_{DIN} is mainly governed by its phase response as its transmissibility in the frequencies investigated is close to one.

For each signal the error in the peak velocities recorded by each seismograph with respect to S_{DIN} is calculated to assess whether they meet the phase response allowed by DIN (it defines that "The actual phase response of the vibration meter may differ from the design phase only so far that the maximum magnitude of two superimposed vibrations does not exceed an error of 20 % in the range 1 Hz to less than 2.5 Hz and an error of 10 % in the range $2.5 \leq f \leq 315$ Hz"). The cases in which this criterion is violated are marked with an arrow in Figure 7. Only seismograph S3 meets this criteria, and probably the maximum deviation allowed is near the phase response of seismograph S2 (it meets this criteria for 13 out of 15 signals).

Seismographs S0, S1 and S2 with steeper phase responses at low frequencies (mainly due to high natural frequencies of their geophones, see Table 1) lead to larger errors. These are more than twice the errors allowed for the phase response suggested by ISEE (which states: "the phase shift between 2.5 to 250 Hz

shall not causes an error of more than 10 % to the maximum value of two superimposed harmonic vibration"; such error is marked with the horizontal black lines in Figure 7). However, it seems that such criterion is very restrictive, as SDIN does not comply with it in four cases (two of them within the range suggested). As one of them occurs for the fundamental frequency of 2.5 Hz, the error at slightly higher fundamental frequency of 3 Hz and its third harmonic has been investigated, resulting in similar values. The fact that the amplitude response suggested by ISEE can decay from 4 and 125 Hz (upper graph, Figure 6) encompass large errors, as the resulting phase shift is large at low and high frequencies, see for instance the responses of seismographs S0 and S1.

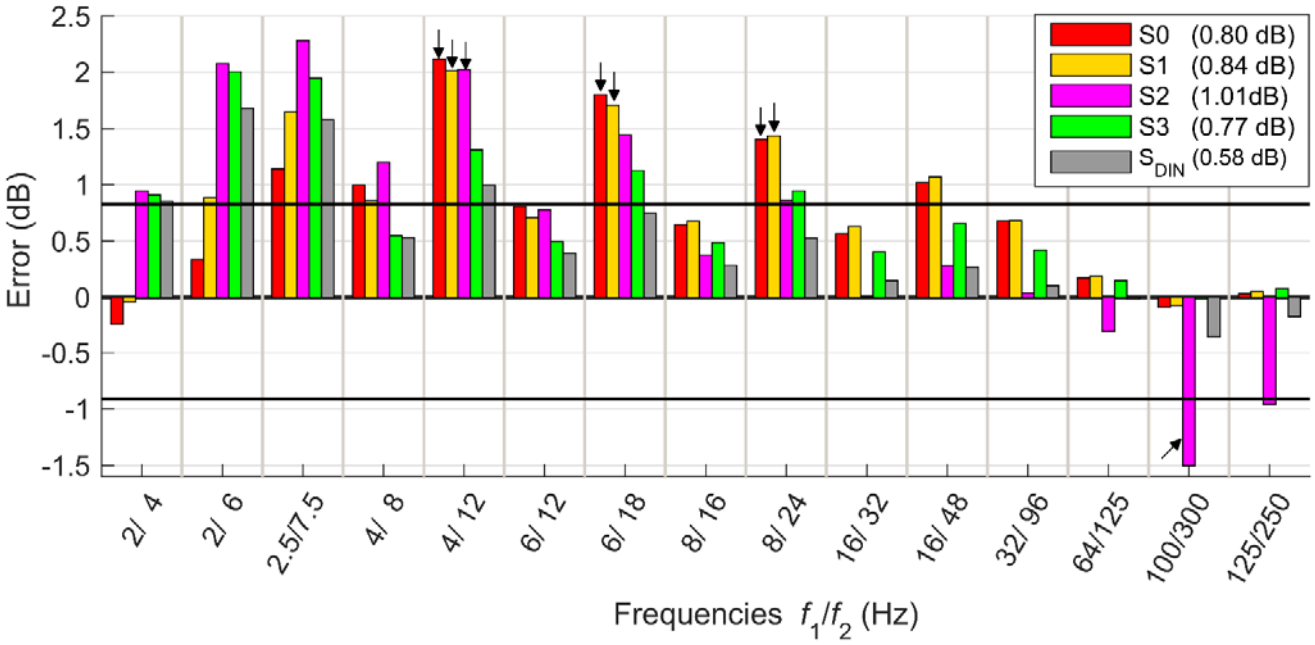

Figure 7. Error-gain in peak velocity for five seismographs measuring two superimposed harmonic vibrations of the same amplitude of different frequencies (0 dB means accurate measurements, while *e* of 2 and -1.5 dB indicates a transmissibility of 1.26 and 0.84, respectively).

Conclusions

This work investigates the performance of seismographs used to monitor vibrations from blasting. The transfer properties (transmissibility and phase shift) of the geophone and its processing-recording unit have been measured from 2 to 315 Hz at 10 mm/s (0.4 in/s). The main elements of the seismograph have been modelled using simple second order type transfer functions. The parameters of these functions have been calibrated from nonlinear fitting of the measured frequency response of the geophone and of the full seismograph. The transfer function has been used to compare the tested device with two theoretical seismographs, which amplitude responses are in line with ISEE, and with two more apparatus in compliance with DIN characteristics; one of these devices has the nominal response (amplitude and phase) specified by that standard. A total of 15 theoretical inputs are generated from the sum of two harmonic waveforms of the same amplitude and different frequencies in the bandwidth studied. Each signal is run through the transfer function of each seismograph, and the error (expressed as gain) in the peak velocity assessed. The largest distortions occurred for input signals with frequencies in the low (<32 Hz) or high ranges (>125 Hz), where the mechanical, electronics and digital parts of the seismograph modify the signals.

Seismographs with the nominal transfer function suggested by DIN 45669:1:2010 (i.e. transmissibility about one with limited phase shift in the bandwidth 2–200 Hz) provide the best performance; errors in peak velocity ranged from -0.4 to 1.7 dB (equivalent to transmissibility of 0.96 and 1.22, respectively). Monitoring devices with transmissibility around one in narrow bandwidths, in line with ISEE criteria for the amplitude response, involve large phase shifts at low and higher frequencies. This leads to larger errors ranged from -1.5 to 2.3 dB (transmissibility of 0.84 to 1.3, respectively). Further research is ongoing to assess the effect (transient and steady-state response) of the apparatus on non- periodic transient vibrations typical form blasting.

Acknowledgments

The authors are grateful to MAXAM Civil Explosives and VIBRAQUIPO for the financial support of the experimental work.

References

AENOR, 1993, "Control de vibraciones producidas por voladuras", Norma UNE 22-381-93, Asociación Española de Normalización y Certificación, Madrid.

BSI, 1993, "Evaluation and measurement for vibration in buildings: Guide to damage levels from groundborne vibration", BS 7385: part 2, British Standard Institution, London.

Chen, C. T., 1995, "Analog and digital control system design: transfer-function, state-space, and algebraic methods", Oxford University Press, Inc., p. 475.

Dowding, C.H., Hamdi, E., Aimone-Martin, C.T, 2016, "Strains induced in urban structures by ultra-high frequency blasting rock motions: A case study", *Rock Mechanics and Rock Engineering*, 1-18.

DIN, 1999, "Structural Vibration– Part 3: Effects of vibration on structures", DIN 4150-3:1999-02, Deutsches Institut für Normung, Berlin.

DIN, 2010, "Measurement of vibration immission–Part 1: Vibration meters −Requirements and tests", DIN 45669−1:2010-09, Deutsches Institut für Normung, Berlin.

Drijkoningen, G.G., 2003, "Seismic data acquisition", Delft University of Technology, Delft, p.43-44.

Farnfield, R.A., "So you think you are monitoring peak particle velocity?", Proc.12th Symposium on Explosives and Blasting Research, 1996, International Society of Explosives Engineers, Cleveland, p. 13-17

Fogelson, D. E., Johnson, C. F., 1962. "Calibration studies of three portable seismographs", Vol. 6009. US Dept. of the Interior, Bureau of Mines.

Havskov, J., Alguacil, G., 2004, "Instrumentation in earthquake seismology", Modern Approaches in Geophysics, Vol. 22, Springer, Netherlands, p. 15-24.

Hutt, C. R., Evans, J. R., Followill, F., Nigbor, R. L., Wielandt, E., 2009, "Guidelines for standardized testing of broadband seismometers and accelerometers", US Geolological Survey, Open-File Report 1295.

ISEE, 2011, "Performance specifications for blasting seismographs", Eltschlager K.K. (standards chairman committee), International Society of Explosives Engineers, Cleveland.

ISO, 2003, "Methods for the calibration of vibration and shock transducers– Part 21: Vibration calibration by comparison to a reference transducer", ISO 16063-21:2003(E).

MATLAB Release 2015b, 2015, The MathWorks, Inc., Masschusetts.

Nanometrics, 2009, "Trillium 40 Seismomemter User guide", Nanometics, Ontario.

Nofal, H., Mohamed, O., Mohanna, M., El-Gabry, M., 2015, "Assessment of the accuracy and stability of ENSN sensors responses", *NRIAG Journal of Astronomy and Geophysics*, 4(1): 48-54.

Orfanidis, S. J., 1995, “Introduction to signal processing”, Prentice-Hall, Inc., P-229-241.

Segarra, P., Sanchidrián, J. A., Castedo, R., López, L. M., del Castillo, I, 2015a, “Performance of some coupling methods for blast vibration monitoring”, *Journal Applied Geophys* (112): 129–135.

Segarra, P., Sanchidrián, J. A., del Castillo I., Castedo, R., López, L. M., “Rock-to-sensor transmissibility of vibrations–Part 2”, Proc. 41st Annual Conf. on Explosives and Blasting Technique, 2015b, International Society of Explosives Engineers, Cleveland

Siskind, D.E., Stagg, J., Kopp, J.W., Dowding C.H., 1980, “Structure Response and Damage Produced by Ground Vibrations from Surface Mine Blasting”, USBM Report of Investigation 8507, United States Bureau of Mines, Twin Cities.

Stagg, M. S., Engler, A. J., 1980, “Measurement of blast-induced ground vibrations and seismograph calibration”, US Department of the Interior, Bureau of Mines.

Telford, W. M., Geldart, L. P., Sheriff, R. E., 1990. “Applied geophysics”, 2nd Edition, Cambridge University Press, p.197-198.

Wielandt, E.,2002, “Seismic sensors and their calibration”, New Manual of Seimsological Observatory Practices.

Udías, A., Madariaga, R., Buforn, E., 2014, “Source Mechanisms of Earthquakes: Theory and Practice”. Cambridge University Press: 22-26.

Ueno, T., Saito, T., Shiomi, K., Haryu, Y., 2015, “Monitoring the instrument response of the high-sensitivity seismograph network in Japan (Hi-net): effects of response changes on seismic interferometry analysiss”, *Earth, Planets and Space*, 67(1): 1-10.